ACS Catalysis

Article

Semi-rational Design of Fluoroacetate Dehalogenase RPA1163 for Kinetic Resolution of #-Fluorocarboxylic Acids on Gram-scale

Hongxia Zhang, Shaixiao Tian, Yue Yue, Min Li, Wei Tong,
Guang-Yu Xu, Bo Chen, Ming Ma, Yanwei Li, and Jian-bo Wang

ACS Catal., **Just Accepted Manuscript** • DOI: 10.1021/acscatal.9b04804 • Publication Date (Web): 03 Feb 2020

is published by the American Chemical Society. 1155 Sixteenth Street N.W., Washington, DC 20036

Semi-rational Design of Fluoroacetate Dehalogenase RPA1163 for Kinetic Resolution of α-Fluorocarboxylic Acids on Gram-scale

Hongxia Zhang[1,3,§], Shaixiao Tian[1,3,§], Yue Yue[4], Min Li[1,3], Wei Tong[1,3], Guangyu Xu[1,3], Bo Chen[1,3], Ming Ma[1,3], Yanwei Li*[,4], and Jian-bo Wang*[,1,2,3]

[1]Key Laboratory of Phytochemistry R&D of Hunan Province, College of Chemistry and Chemical Engineering, Hunan Normal University, Changsha 410081, People's Republic of China.

[2]State Key Laboratory of Biocatalysis and Enzyme Engineering, Hubei Collaborative Innovation Center for Green Transformation of Bio-resources, Hubei Key Laboratory of Industrial Biotechnology, School of Life Sciences, Hubei University, 368 Youyi Road, Wuchang Wuhan, 430062, People's Republic of China.

[3]Key Laboratory of Chemical Biology and Traditional Chinese Medicine Research (Ministry of Education), College of Chemistry and Chemical Engineering, Hunan Normal University Changsha 410081, People's Republic of China.

[4]Environment Research Institute, Shandong University, Qingdao 266237, People's Republic of China.

ABSTRACT: Here the synthetic utility of fluoroacetate dehalogenase RPA1163 is explored for the production of enantiomerically pure (*R*)-*α*-fluorocarboxylic acids and (*R*)-*α*-hydroxylcarboxylic acids via kinetic resolution of racemic *α*-fluorocarboxylic acids. While wild-type (WT) RPA1163 shows high thermostability and fairly wide substrate-scope, many interesting, yet poorly or moderately accepted substrates exist. In order to solve this problem and to develop up-scaled production, *in silico* calculations and semi-rational mutagenesis were employed. Residue W185 was engineered to alanine, serine, threonine or asparagine. The two best mutants W185N and W185T showed significantly improved performance in the reactions of these substrates, while *in silico* calculations shed light on the origin of these improvements. Finally, 10 *α*-fluorocarboxylic acids and 10 *α*-hydroxycarboxylic acids were prepared on gram-scale via kinetic resolution enabled by WT, W185T or W185N. This work expands the biocatalytic toolbox and allows a deep insight into the fluoroacetate dehalogenase catalyzed C-F cleavage mechanism.

KEYWORDS: Semi-rational enzyme design, fluoroacetate dehalogenase, kinetic resolution, α-fluorocaoboxylic acids, α-hydroxy-carboxylic acids.

INTRODUCTION

Since the incorporation of fluorine often induces remarkable changes of physical and biological properties of many organic compounds, organofluorines have been studied in a variety of fields, especially as agrochemicals and pharmaceuticals.[1,2] Among them, *α*-fluorocarboxylic acids (FCAs) have attracted considerable attention due to their inherent bioactivities and utility as building blocks in the construction of more complex pharmaceutical molecules.[3-5] The demand for these compounds calls for the fast development of synthetic methodologies. To date, FCAs can be obtained via nucleophilic substitution and electrophilic addition,[1,6-10] or by C-C bond forming reactions of *α*-fluorocarbonyl compounds.[6-11] However, enantioselective introduction of fluorine into the *α*-position of FCAs remains challenging. Asymmetric synthesis and chiral resolution are two common approaches to produce enantio-pure FCAs. Asymmetric synthesis usually requires metal-catalysts or organic reagents for enolization of the substrate, and organic solvents are indespensible.[6,8,12-26] In contrast, reports about converting easy-access FCAs as racemates into enantio-pure products via chiral resolution are rare. In general, kinetic resolution using man-made catalysts is a facile method to obtain enantio-pure compounds, because it not only affords the target enantiomer, but also creates a new structurally different enantio-pure product. This increases the diversity of products without any waste. Biocatalyts present competitive process to the chemical catalysts due to their excellent selectivities (enantio-, regio-, and chemo). However, their own properties such as stabilities, specificities and catalytic efficiencies have hampered their wide application. With the technical development of molecular biology and bioinformatics, drawbacks of biocatalysts can be overcome by appropriate tools such as enzyme mining, directed evolution, compute-assisted rational design and so on. As a result, biocatalysts are gaining more and more attention and enzymatic kinetic resolution plays an important role in producing enantiomerically pure compounds in this field.[27-32] However, in preparing enantio-pure FCAs by the biocatalytic method, to the best of our knowledge, the most recent report

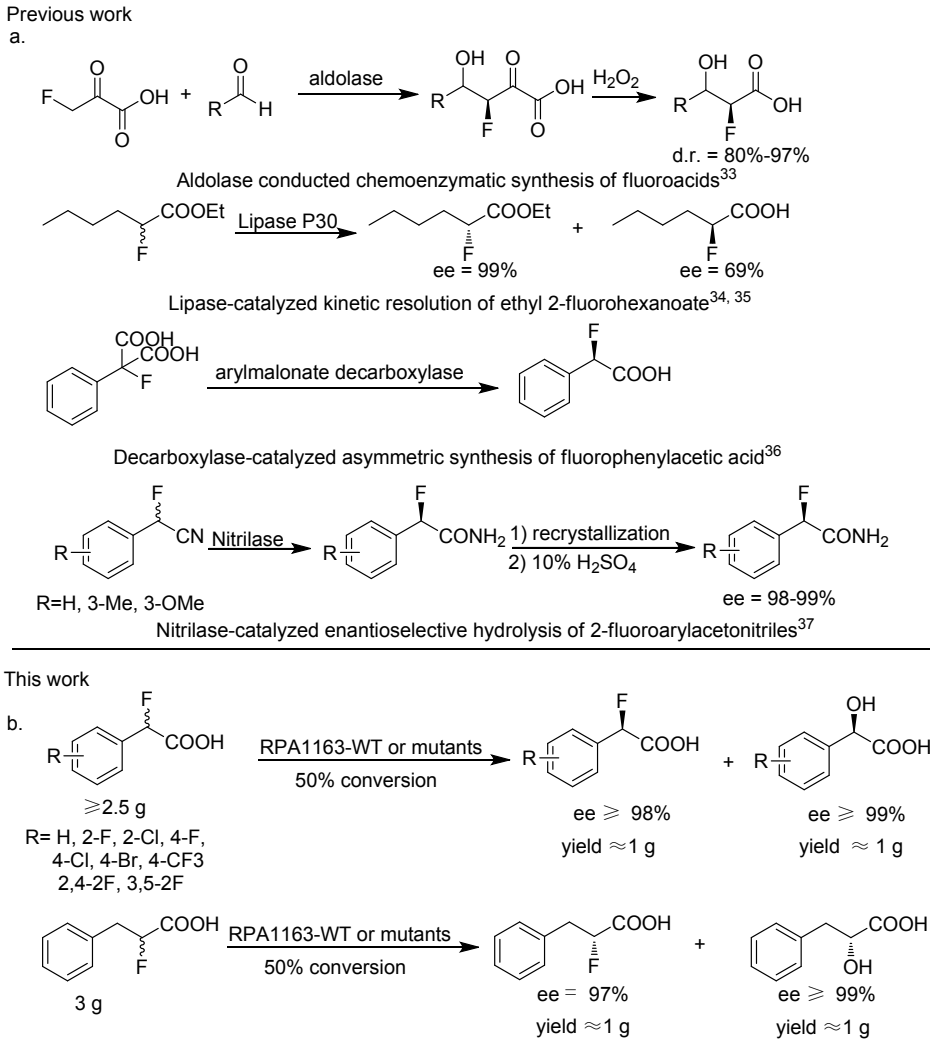

SCHEME 1. Biocatalytic strategies to produce enantio-pure α-fluorocarboxylic acids. a. Aldolase, lipase, nitrilase and malonate decarboxylase-catalyzed production of enantio-pure α-fluorocarboxylic acids. b. WT and mutants of RPA1163 as catalysts in the production of enantio-pure 2-fluorocarboxylic acids and 2-hydroxycarboxylic acids.

concerns chemoenzymatic synthesis of FCAs via aldolase-catalyzed fluoropyruvate addition to diverse adehydes,[33] which complements previous aldol-catalyzed reactions.[11] Research prior to these developments was restricted to the use of carboxylic acid derivatives such as carboxylic acid esters,[34,35] dicarboxylic acids,[36] and nitriles[37] as substrates (**Scheme 1a**). Even in these cases, the drawbacks often include narrow substrate-scope or difficulties in implementing large scale preparations.

Fluoroacetate dehalogenase RPA1163 was first isolated and identified from *Rhodopseudomonas palustris* CGA009 in 2010.[38] It attracts attention due to its ability to cleave the very strong σ-C-F bond under mild conditions. Studies concerning the catalytic mechanism have been performed by protein crystal structure resolution[39-41] and computational modeling.[42-45] The results suggest that RPA1163 employs a similar carbon-halide bond cleavage mechanism as *L*-2-haloacid dehalogenase,[46] having an Asp-His-Asp triad that catalyzes the substitution of fluoride by hydroxyl via an S_N2 mechanism. Nevertheless, hitherto investigations of this enzyme focused on clarifying the mechanism and identifying key residues related to the basic catalytic activity, while its potential synthetic applications remain underappreciated. Moreover, which residues influence activity and stereoselectivity most effectively was also not fully clear. Our prior investigation disclosed (*S*)-enantioselectivity of wild-type (WT) RPA1163 when 2-fluorophenyl acetic acid and 2-fluorophenyl propionic acid were used as substrates,[47] this mechanistic probe indicating its potential synthetic utility for producing enantio-pure FCAs in general.

Here, with the computer-aided design, the activity of RPA1163 toward a number of substrates was significantly enhanced via semi-rational mutagenesis. Based on its excellent catalytic property, we explored a new utilization of RPA1163 for producing enantio-pure (*R*)-FCAs on gram-scale via kinetic resolution (**Scheme 1b**). This work not only provides a highly efficient and (*R*)-selective pathway to two types of enantio-pure compounds (FCAs and *α*-hydroxylcarboxylic acids), but also promotes the mechanistic insight of the C-F bond cleavage

mechanism enabled by this type of enzyme. Finally, our study highlights the precision of computer aided enzyme engineering.

RESULTS AND DISCUSSION

Thermostability test and optimization of reaction conditions. While nine years has past since RPA1163 was reported[38] for the first time, no work has been published to characterize its thermostability and to optimize its reaction conditions. To test its thermostability, we incubated the purified enzyme at different temperatures for 30 minutes, and then tested its activity in the defluorination of α-fluorophenyacetic acid (**1a**). Surprisingly, the results showed that RPA1163 endures temperatures as high as 70 °C without significant activity-loss (**Figure S2a**). It can even maintain half of its activity when the temperature was increased further to 84 °C. Moreover, upon keeping the RPA1163-containing *E. coli* whole cells at room temperature (about 25 °C) for 10 days, no activity loss can be detected (**Figure S2b**). Encouraged by these results, we optimized the reaction conditions by adjusting temperature and pH. As shown in Figure 1a and Figure 1b, highest activity is observed at 60 °C and pH 7.0.

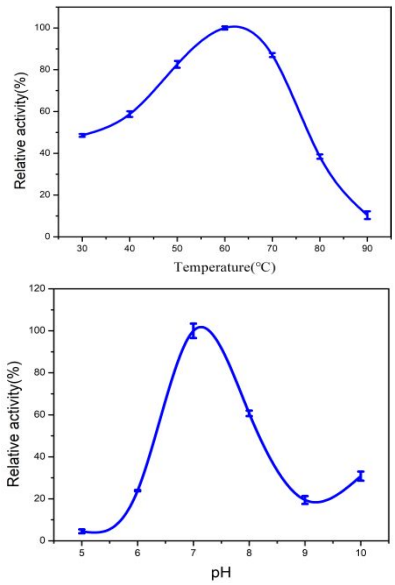

Figure 1. Optimization of temperature and pH of RPA1163 as a catalyst in the reaction of substrate 1a. a. Optimization of reaction temperature; b. Optimization of reaction pH.

Exploration of Substrate Scope. Thus far only limited types of substrates have been tested using RPA1163.[47] To explore the substrate-scope of the WT, 10 compounds were tested under the optimized conditions (**SCHEME 2**). Purified RPA1163 was employed in all reactions, turnover numbers (TON) being calculated based on the consumption of substrates. As Table 1 shows, with the exception of compounds **1h** and **1i**, WT is very active toward most of the substrates. The huge difference in activity upon going from substrate **1g** to **1h** by a factor of 76 is remarkable, because the difference in size is only moderate.

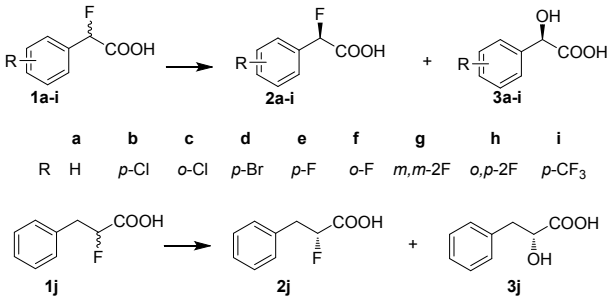

SCHEME 2. Exploring the substrate-scope of RPA1163.

Table 1. TON data for all of the tested substrates catalyzed by WT RPA1163. Heterolytic BDE is the C-F bond dissociation energy calculated at M06-2x/6-311++G(3df,3pd) level.

Substrate	Heterolytic BDE (kcal/mol)	TON (WT)
1a	85.5	566500
1b	95.9	19573
1c	89.6	39773
1d	96.6	31613
1e	93.7	39300
1f	88.0	42500
1g	104.5	69410
1h	87.5	913
1i	104.1	1339
1j	102.1	75375

Mechanistic investigation. Why is the activity of **1h** 76 times lower than **1g**? Here we raise three speculations. First, the intrinsic properties of substrates such as stronger C-F bond strength may lead to the low activity. In order to test this possibility, DFT calculations at M06-2x/6-311++g (3df, 3pd) level were performed for determining the heterolytic bond dissociation energy (BDE) of C-F bond. The results show that the respective heterolytic BDE of **1h** is not the largest among the 10 explored compounds (**Table 1**). Actually, the heterolytic BDE of **1h** is even 17.0 kcal mol^{-1} lower than that of **1g**. Together with the fact that C-F bond cleavage has been confirmed to be fast,[39, 42-48] this possibility was excluded. Second, the low activity toward **1h** may result from low enzyme binding affinity. To verify this speculation, kinetic tests were conducted for all substrates (**Table 2**). Upon comparing the K_m value of **1g** with that of **1h**, and considering the case of **1a** versus **1i**, substrates with low activities actually have small K_m values. Thus, we conclude that the binding affinity is not the determining factor. The third explanation was tested by analyzing the kinetics data. We found that the k_{cat}-value of **1g** is 518-fold larger than that of **1h**. Therefore, we conclude that the higher energy barrier of the rate-limiting step causes the lower activity. It is well-known that the fluoroacetate dehalogenase catalyzed defluorination includes three major steps: (**I**) Aspartic acid attacks the C-F bond and fluoride anion is liberated; (**II**) histidine deprotonates the water molecule, the activated hydroxyl group then attacks the aspartic acid's carbonyl function to form an intermediate with the (*R*)-

configuration at the α-C position due to the strict (*S*)-enantioselectivity and proven S_N2 mechanism);[47] (**III**), while the protonated histidine feeds the proton back to the intermediate and induces C-O cleavage (**Figure 2** and **Movie S1**). We performed WT-catalyzed defluorination of **1g** and **1h** in D_2O to try to clarify whether step **I** is the rate-determining step. However, the experimental results show that kinetic isotope effects (KIEs) in reactions of these two substrates are close to 1 (**Table S2**, 1.07 for **1g** and 0.97 for **1h**). A theoretical calculation was also performed to assess the KIE-values of these two substrates, which verified our experimental results again (**Table S3**), both KIE-values are 1. Since step **I** cannot be excluded by the isotope experiment, we chose to trust previous work which confirmed that step **I** is very fast.[39,42-45,48] Moreover, during the submission of this work, the Pai group presented the whole process of RPA1163-catalyzed defluorination of fluoroacetic acid via time-solved crystallography,[49] which clearly showed that step **I** is more quick than the other two steps (200 ms vs 2 s). Nevertheless, they did not distinguish between step **II** and step **III**. At this point, the next work is to evaluate the remaining two steps and to find out which one is rate-determining.

For this purpose, quantum mechanics/molecular mechanics (QM/MM) calculations were applied to obtain the energy barriers for step **II** and step **III.** The robustness and accuracy of the QM/MM method has been demonstrated by many other groups.[50-55] Optimized at B3LYP/6-31G(d,p)//CHARMM22 level, in the case of **1h**, the structures show that step **II** is achieved with the aid of histidine 280. The corresponding energy barrier is 25.4 kcal mol^{-1} at RIMP2/cc-pVTZ//CHARMM22 level (**Figure S3**). Intermediate IM1 is not stable, it easily transforms to the final product through C-O bond cleavage with an energy barrier of only 4.8 kcal mol^{-1}. Thus, step II is the rate-determining step for the fluoroacetate dehalogenase catalyzed transformation of **1h**. In the case of **1g**, there is a change in the rate-determining step where TS2 in step **III** determines the catalytic efficiency. The corresponding energy barrier is 23.5 kcal mol^{-1} (**Figure S3**).[56-57] The higher energy barrier for **1h** than **1g** is in good accordance with the corresponding lower k_{cat} values. In addition, one more kinetic

Table 2. Kinetic test of RPA1163 WT in reactions of all substrates

substrate	K_m (mM)	k_{cat} (min^{-1})	k_{cat}/K_m ($mM^{-1}*min^{-1}$)
1a	2.4±0.5	676.3±29.0	281.8
1b	3.3±0.6	30.4±1.5	9.2
1c	3.2±0.6	35.5±1.6	11.0
1d	0.7±0.4	17.1±1.0	19.4
1e	2.7±0.5	24.9±1.1	9.2
1f	1.5±0.3	40.5±1.4	27.4
1g	5.9±1.3	1036.0±82.0	175.6
1h	4.0±0.5	2.9±0.8	0.7
1i	1.4±0.2	10.4±0.4	7.6
1j	3.1±0.7	49.6±0.5	16.0

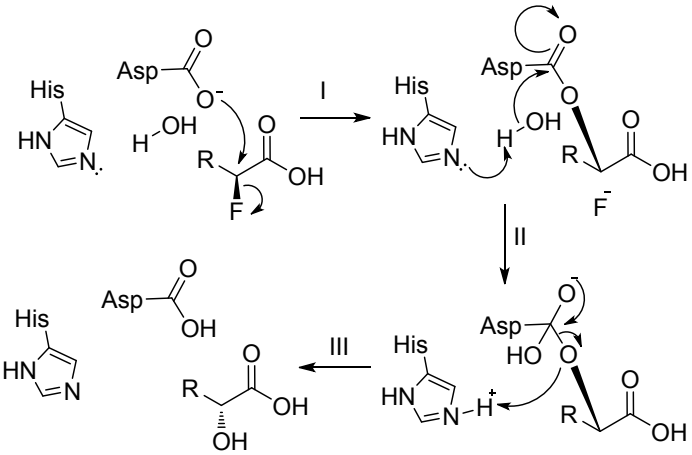

Figure 2. The mechanism of fluoroacetate dehalogenase catalyzed defluorination.

test with 2-fluoro-2-(4-methylphenyl)acetic acid (**1k**) was performed (k_{cat}=149.7±6.1, *K*m=3.3±0.5) and a Hammett plot based on $\log(k_{cat,\mathbf{1b\text{-}1k}}/k_{cat,\mathbf{1a}})$ vs σ was created. The result shows two types of linear fit that substrates with a *p*-substitution (e.g. **1h**) have a ρ value of -1.85 while substrates without *p*-substitution (e.g. **1g**) have a quite different ρ value of -1.15 (**Figure S4**). This supports a change of the rate-determining step between **1h** and **1g**.

Semi-rational Design of RPA1163 Mutants for Challenging Substrates. To construct a high-efficiency RPA1163 mutant for such challenging substrates as **1h**, semi-rational design was applied. As we previously mentioned,[47] RPA1163 shows strict (*S*)-selectivity due to the rather lower ligand binding energy for (*S*)-enantiomers as opposed to the (*R*)-enantiomers. Here, we also found that WT displays essentially complete (*S*)- enantioselectivity for **1h**. Consequently, (*S*)-**1h** was docked into the active pocket of RPA1163, and a limited selection of mutants at 16 residues within 5 Å of **1h** were screened and analyzed (**Figure S5**). According to previous reports,[39,42,48] RPA1163 is well evolved and most of its residues near the active site proved to be vital for catalysis and resistant to mutation, thus residues like D110, R111, R114, D134, H155, W156, Y219 and H280 were ruled out. Subsequently, analysis of structural parameters influencing the rate-determining step (step **II**) shows that the dihedral angle between the plane of benzyl in substrate **1h** and the plane of C_α-O (DA) and the angle between C_{benzyl}-C_α and C_α-O (Ang) are only 62.4° and 106.3° in WT, which deviates substantially from the corresponding values in solution (112.2° and 107.3°) and the final product (114.3° and 111.4 °). As indicated in Figure 3a, the large size residue W185 was identified as the major cause for the suboptimal conformation of **1h** in WT. Therefore, reducing the size of residue W185 should reduce compactness and enhance enzymatic activity. Rather than performing tedious saturation mutagenesis, we first computationally designed the W185A mutant where large tryptophan was mutated to the smallest nonpolar amino acid, alanine (**Figure 3b**). The DA and Ang increase by 20.2° and 3.3° in W185A. In addition, the distance between the phenyl group of **1h** and imidazole group of H280 also increase from 4.8 Å in WT to 5.1 Å in mutant W185A. The long distance can be expected to decrease the ∏---∏ stacking interaction and to prompt the fast release of product. For the complexity

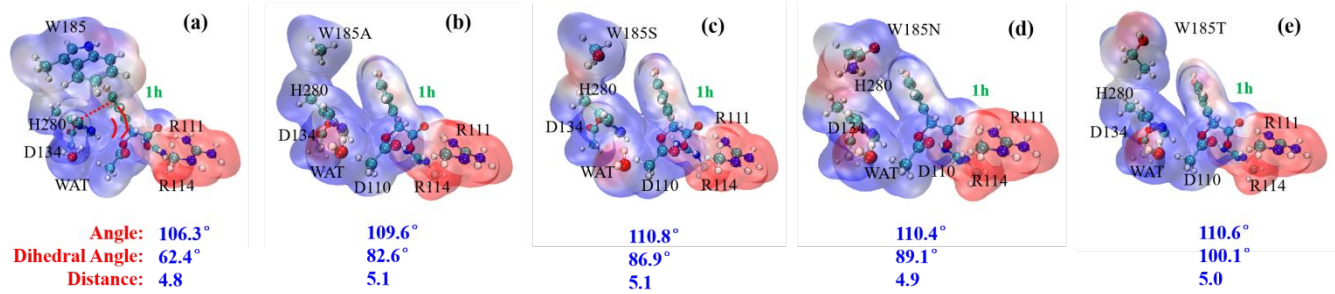

Figure 3. Key structural parameters and electrostatic potential surface of the RPA1163 active site with substrate 1h. Panels a~e are the reactants (R) of the nucleophilic attack step for WT, W185A, W185S, W185N and W185T. As shown in panel a, angle C_{benzyl}-C_{α}-O is indicated in red arc, dihedral angle between the plane of benzyl in substrate 1h and the plane of C_{α}-O is indicated in red polyline, distance between the phenyl group of 1h and imidazole group of H280 is indicated by dotted line.

of enzymatic reaction, the geometric size is often not the only determined factor, other interactions such as electrostatic force and hydrogen bonds must be taken into consideration. Therefore, three polar amino acids (serine, threonine and asparagine) with similar size as alanine were also computationally screened. As indicated in Figure 3c~3e, the analyzed structural parameters consistently show increased fitting for **1h** in W185S, W185N and W185T mutants relative to WT. Larger DA and Ang support product formation. Furthermore, electrostatic potential surface analysis highlights a stronger interaction between W185 and **1h** in WT than in mutants (W185A, W185S, W185N, W185T). The mutations allow substrates to enter more efficiently and products to depart faster, thus resulting in higher catalytic efficiency. Considering the different DA-values among 4 mutants, it looks like W185N and W185T should be the two best mutants toward substrate **1h**. *In vitro* verification was performed with W185 mutated to alanine, serine, threonine and asparagine. All mutants were expressed and purified after confirmation by sequencing. Activities and enantioselectivities were determined by gas chromatography (GC). As we predicted, all mutants exhibited higher activities than WT. Not surprisingly, W185N and W185T proved to be the two best ones toward **1h** (**Figure S6**). To confirm the origin of the activity increase in W185N and W185T mutants, kinetic experiments were performed (**Table 3**). In these cases, the results showed that K_m in reactions of either **1h** or **1i** for both of the mutants remained constant or increased only slightly, while the k_{cat} values significantly increased by 16- and 19-fold, respectively. Our QM/MM results (**Figure 4 and Figure S7**) confirm that the mutations in variants W185N and W185T decrease the energy barrier by 3.6 and 2.3 kcal mol^{-1}, respectively. Thus, both *in silico* computations and *in vitro* experiments suggest that it is not the binding affinity, but the catalytic k_{cat} values that rule the overall activity.

Table 3. Kinetic test of RPA1163 mutants W185N and W185T in reactions of 1h and 1i.

RPA1163 variants	substrate	K_m (mM)	k_{cat} (min^{-1})	k_{cat}/K_m (mM^{-1}*min^{-1})
W185N	**1h**	3.1±0.4	55.4±1.5	17.9
W185T	**1h**	2.2±0.6	47.2±2.6	21.5
W185N	**1i**	3.8±1.5	1239.0±151.0	326.0
W185T	**1i**	6.2±1.5	1537.0±164.0	248.0

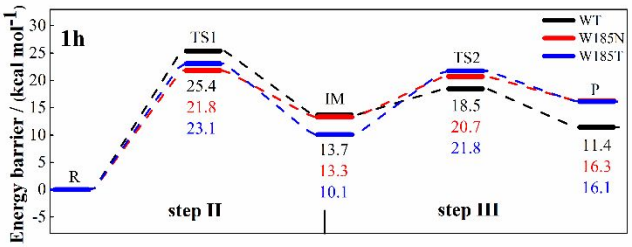

Figure 4. Potential energy profiles for the RPA1163 WT, W185N and W185T catalyzed reactions of 1h calculated at RIMP2/cc-pVTZ//CHARMM22 level.

Interestingly, W185 has also been assumed to function as a lid to control the entry of substrates and departure of products from the binding pocket.[39] Here, 1000 ns molecular dynamics (MD) simulations for WT, W185N and W185T were performed. As indicated in Figure 5, the MD simulations show that WT has the narrowest entry (d1=4.7 Å, d2=5.8 Å) for substrate or product compared with W185N and W185T mutants in 0~100 ns. The tunnel becomes more open (d1=7.6 Å, d2=8.8 Å) when the simulation time is extended to 1000 ns, which indicates that large loop motions occur. In contrast, the entries of W185N and W185T mutants are wider and stay stable during the whole 1000 ns simulation. Clearly, in the case of WT, large loop motions are needed for association and disassociation, which requires an additional energy input compared to the mutants. To confirm whether this motion affects the association and dissociation of substrate and product, tests of kinetic solvent viscosity effects (KSVEs)[58] (**Figure S8**) were performed for **1g** and **1h**. All reactions were performed in different concentrations of glycerol, and the K_m and k_{cat} values were determined in each condition. Then two plots were created based on $(k_{cat}/K_m)_0$ /$(k_{cat}/K_m)_\eta$ versus η/η_0(plot a) and $(k_{cat})_0/(k_{cat})_\eta$ versus η/η_0 (plot b). Their slopes indicate whether the reaction is affected by the association of substrate or the dissociation of product. For **1g**, the slopes in plots of $(k_{cat}/K_m)_0/(k_{cat}/K_m)_\eta$ versus η/η_0 and $(k_{cat})_0/(k_{cat})_\eta$ versus η/η_0 are 0.2 and 0.3 respectively. These values are in the range of 0-1, which indicates that the activity for **1g** is partially inhibited by the capture of the substrate and by the release of the product. For **1h**, slopes in plots of $(k_{cat}/K_m)_0/(k_{cat}/K_m)_\eta$ VS η/η_0 and $(k_{cat})_0/(k_{cat})_\eta$ VS η/η_0 are 0 and 0.2, respectively. These results indicate that the activity is not affected by the association of substrate, rather, it is partially limited by the dissociation of product. Considering the activity of

WT toward **1g** is rather higher then toward **1h**, we can conclude energy

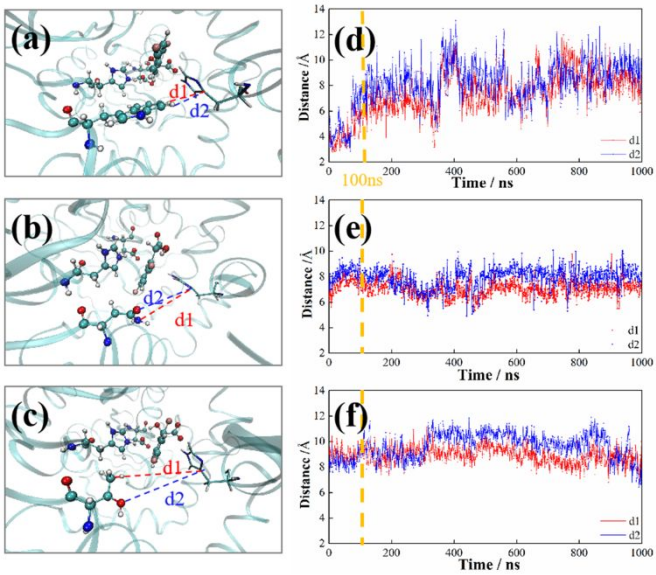

		WT	W185N	W185T
0~100 ns	d1	4.7±1.9	7.1±1.5	9.2±1.2
	d2	5.8±2.9	8.2±1.3	8.7±1.1
100~1000 ns	d1	7.6±4.4	7.6±2.2	9.0±2.2
	d2	8.8±4.3	7.5±2.6	9.2±2.7

Figure 5. Effect of RPA1163 mutations W185N and W185T on the channel for substrate entry and product departure. Panels a~c are the structures of the channels in WT, W185N and W185T. Distances d1 and d2 are selected key distances between W185/W185N/W185T and H155. Panels d~f are distance variations along 1000 ns MD simulations. The values of distances are shown in Å.

Table 4. TON data for all of the tested substrates catalyzed by W185N and W185T.

Substrate	TON (W185N)	TON (W185T)
1a	737870	497744
1b	60600	67950
1c	37350	21225
1d	480112	546750
1e	137850	141150
1f	125458	89821
1g	106728	60421
1h	13650	10348
1i	9944	22275
1j	51784	25191

barrier plays a dominant role to determine the catalytic efficiency. The MD findings, QM/MM results and experimental results together also highlight the benefit of mutating W185 to asparagine or threonine.

Based on the above positive results, a new synthetic strategy for the preparation of (2*R*)-fluorocarboxylic acids and (2*R*)-hydroxylcarboxylic acids was ready for practical testing. We tested all the substrates with the best mutants W185N and W185T. Turnover numbers (TON) were calculated based on the consumption of substrates (**Table 4**). Most mutants exhibit good activity. Especially, mutant W185T was found to exhibit at least a 2-fold enhancement of activity toward moderately active substrates and even a 20-fold activity increase in the case of substrate **1i**.

Substrate-scope exploration and gram-scale preparations of products. Encouraged by these results, we employed WT RPA1163, variant W185N and W185T as biocatalysts in the preparation of **2a-j** and **3a-j** on gram-scale. For convenient application, all catalysts were used in their whole-cell lysate forms. As summarized in Table 5, excellent results were achieved, high enantio-pure compounds **2a-j** and **3a-j** can be obtained in the second step via column chromatography-based isolation. All reactions were completed within 7 hours, and some of them such as reactions with **1a**, **1b**, **1d**, **1e**, **1g** and **1i** were even finished within 1 hour. In addition, this enzymatic reaction is strictly (*S*)-enantioselective, indeed, extended time do not lead to the conversion of (*R*)-substrates.

CONCLUSIONS

In summary, we have characterized fluoroacetate dehalogenase RPA1163 as a highly thermostable biocatalyst, which is a crucial property for industrial applications. While WT shows low activity toward **1h**, to improve this property, a computer-aided design strategy was performed. We first identified the rate-determining step in the whole catalytic cycle via comparing the energy barrier in each step. Then we analyzed the structural parameters of intermediates in the rate-determining step, the DA and Ang of **1h** were compared when **1h** is in the intermediate or in the solvent. The result showed that W185 is too big to provide sufficient space for accommodating **1h**. Therefore, substituting W185 by small residues seemed appropriate. Consequently, we designed 4 mutants (W185A, W185S, W185T, W185N) not only considering the geometry factor, but also possible electrostatic force and hydrogen bond effects. All mutants were characterized by calculations and experiments, the results demonstrating that the theoretical prediction is very precise. All mutants showed better activity than WT, and the two best mutants, likewise predicted by the calculation, were also confirmed by experiment. And it should be noted, unlike our work in 2017[47], here we have identified a hotspot (W185) by way of semi-rational protein design, and succeeded in achieving a significant improvement of its activity toward most of substrates with a single site mutation, which promoted its application for the kinetic resolution of *α*-fluorocarboxylic acids on gram-scale. Significantly, our *in silico* calculations uncover the rate-determining step of the detailed catalytic process and also predicts future mutational directions. This work provides a facile tool for large-scale preparation of enantio-pure *α*-fluoro and *α*-hydroxy carboxylic acids and deepens our understanding of the mechanism of fluoroacetate dehaogenase-catalyzed C-F activation.

Table 5. Gram-scale preparation of α-fluorocarboxylic acids and α-hydroxylcarboxylic acids

Substrate	Amount of substrate (g)	RPA1163 variants	Catalyst concentration (cdw: g/L)	(*R*)-**2a-2j** ee %	(*R*)-**2a-2j** Yield %	(*R*)-**3a-3j** ee %	(*R*)-**3a-3j** Yield %	Reaction time (h)
1a	3	W185N	10	> 99	96.7 (1.45 g)	> 99	96.4 (1.43 g)	1
1b	3	W185T	10	> 99	64.9 (0.97 g)	> 99	77.7 (1.15 g)	1
1c	2.5	WT	30	98	68.2 (0.86 g)	> 99	74.6 (0.93 g)	6
1d	3	W185T	10	> 99	66.9 (1.00 g)	> 99	87.4 (1.30 g)	1
1e	3	W185T	10	> 99	73.6 (1.11 g)	> 99	90.1 (1.33 g)	1
1f	3	W185N	10	98	68.8 (1.03 g)	> 99	74.2 (1.11 g)	2
1g	3	W185N	10	> 99	82.0 (1.23 g)	> 99	76.9 (1.15 g)	1
1h	3	W185N	20	> 99	58.3 (0.88 g)	> 99	66.0 (0.98 g)	4
1i	3	W185T	10	> 99	82.4 (1.24 g)	> 99	93.0 (1.38 g)	1
1j	3	WT	20	97	64.0 (0.96 g)	> 99	68.8 (1.03 g)	7

ASSOCIATED CONTENT

Supporting Information

The Supporting Information is available free of charge at http://pubs.acs.org."
All chemicals, materials of molecular biology and experimental details.

AUTHOR INFORMATION

Corresponding Author

*Jian-bo Wang: jwang@hunnu.edu.cn
*Yanwei Li: lyw@sdu.edu.cn

Author Contributions

The manuscript was written through contributions of all authors.
All authors have given approval to the final version of the manuscript.
§ These authors contributed equally.

Notes

The authors declare no competing financial interest.

ACKNOWLEDGMENT

J. Wang thanks Hunan Normal University for the start-up funding and the support from Huxiang High-level Talent Gathering Project of Hunan Province (2019RS1040). J. Wang was partially supported by Open Project Funding of the State Key Laboratory of Biocatalysis and Enzyme Engineering SKLBEE2018012. B. Chen and M. Ma acknowledge support from the National Natural Science Foundation of China (21575040, 21775041). Y. Li thanks Young Scholars Program of Shandong University (2018WLJH54) for support.

REFERENCES

(1). Groult, H.; Leroux, F.; Tressaud, A., Eds. *Modern Synthesis Processes and Reactivity of Fluorinated Compounds: Catalytic Enantioselective Fluorination.*; Elsevier: Amsterdam, **2017**, *chapter 9*, 223-263.

(2) Gillis, E. P.; Eastman, K. J.; Hill, M. D.; Donnelly, D. J.; Meanwell, N. A. Applications of Fluorine in Medicinal Chemistry. *J. Med. Chem.* **2015**, *58*, 8315-8359.

(3) Huang, H.; Meegalla, S. K.; Lanter, J. C.; Winters, M. P.; Zhao, S.; Littrell, J.; Qi, J.; Rady, B.; Lee, P. S.; Liu, J. Discovery of a GPR40

Superagonist: The Impact of Aryl Propionic Acid α-Fluorination. *ACS Med. Chem. Lett.* **2018**, *10*, 16-21.

(4) Lin, G.; You, Q.; Cheng, J., Eds. *Chiral Drugs: Fluoring-containing Chiral Drugs.*; Wiley: Hoboken, NJ, **2011,** *chapter 5*, 195-251.

(5) Zhang, Y.-K.; Plattner, J. J.; Freund, Y. R.; Easom, E. E.; Zhou, Y.; Ye, L.; Zhou, H.; Waterson, D.; Gamo, F.-J.; Sanz, L. M. Benzoxaborole Antimalarial Agents. Part 2: Discovery of Fluoro-substituted 7-(2-carboxyethyl)-1, 3-dihydro-1-hydroxy-2, 1-benzoxaboroles. *Med. Chem. Lett.* **2012**, *22*, 1299-1307.

(6) Liang, T.; Neumann, C. N.; Ritter, T. Introduction of Fluorine and Fluorine-Containing Functional Groups. *Angew. Chem. Int. Ed.* **2013**, *52,* 8214-8264.

(7) Champagne, P. A.; Desroches, J.; Hamel, J.-D.; Vandamme, M.; Paquin, J.-F. Monofluorination of Organic Compounds: 10 Years of Innovation. *Chem. Rev.* **2015**, *115*, 9073-9174.

(8) Gray, E. E.; Nielsen, M. K.; Choquette, K. A.; Kalow, J. A.; Graham, T. J.; Doyle, A. G. Nucleophilic (Radio) Fluorination of α-Diazocarbonyl Compounds Enabled by Copper-Catalyzed H-F Insertion. *J. Am. Chem. Soc.* **2016**, *138*, 10802-10805.

(9) Saadi, J.; Wennemers, H. Enantioselective Aldol Reactions with Masked Fluoroacetates. *Nat. Chem.* **2016**, *8*, 276.

(10) Minhas, H. K.; Riley, W.; Stuart, A. M.; Urbonaite, M. Activation of the Hypervalent Fluoroiodane Reagent by Hydrogen Bonding to Hexafluoroisopropanol. *Org. Biomol. Chem.* **2018**, *16,* 7170-7173.

(11) Li, Y. L.; Wang, X. L.; Xiao, D.; Liu, M. Y.; Du, Y.; Deng, J. Organocatalytic Biomimetic Decarboxylative Aldol Reaction of Fluorinated β-Keto Acids with Unprotected Isatins. *Adv. Synth.Catal.* **2018**, *360,* 4147-4152.

(12) Zhang, L.; Luo, S. Reagent-controlled Enantioselectivity Switch for the Asymmetric Fluorination of β-Ketocarbonyls by Chiral Primary Amine Catalysis. *Chem. Sci.* **2017**, *8,* 621-626.

(13) Xu, Y.-S.; Tang, Y.; Feng, H.-J.; Liu, J.-T.; Hsung, R. P. A. Highly Regio-and Stereoselective Synthesis of α-Fluorinated Imides via Fluorination of Chiral Enamides. *Org. Lett.* **2015**, *17,* 572-575.

(14) Yang, X.; Wu, T.; Phipps, R. J.; Toste, F. D. Advances in Catalytic Enantioselective Fluorination, Mono-, Di-, and Trifluoromethylation, and Trifluoromethylthiolation Reactions. *Chem. Rev.* **2014**, *115,* 826-870.

(15) Lee, S. Y.; Neufeind, S.; Fu, G. C. Enantioselective Nucleophile-catalyzed Synthesis of Tertiary Alkyl Fluorides via the α-Fluorination of Ketenes: Synthetic and Mechanistic Studies. *J. Am. Chem. Soc.* **2014**, *136*, 8899-8902.

(16) Hintermann, L.; Perseghini, M.; Togni, A. Development of the Titanium–TADDOLate-Catalyzed Asymmetric Fluorination of β-Ketoesters. *Beilstein, J. Org. Chem.* **2011**, *7*, 1421-1435.

(17) Smith, A. M.; Hii, K. K. Transition Metal Catalyzed Enantioselective α-Heterofunctionalization of Carbonyl Compounds. *Chem. Rev.* **2010**, *111*, 1637-1656.

(18) Kawatsura, M.; Hayashi, S.; Komatsu, Y.; Hayase, S.; Itoh, T. Enantioselective α-Fluorination and Chlorination of β-Ketoesters by Cobalt Catalyst. *Chem. Lett.* **2010**, *39*, 466-467.

(19) Duggan, P. J.; Johnston, M.; March, T. L. Enantioselective Synthesis of α-Fluoro-β^3-amino Esters: Synthesis of Enantiopure, Orthogonally Protected α-Fluoro-β^3-lysine. *J. Org. Chem.* **2010**, *75*, 7365-7372.

(20) Cahard, D.; Xu, X.; Couve-Bonnaire, S.; Pannecoucke, X. Fluorine & Chirality: How to Create a Nonracemic Stereogenic Carbon–Fluorine Centre? *Chem. Soc. Rev.* **2010**, *39*, 558-568.

(21) Erb, J.; Alden-Danforth, E.; Kopf, N.; Scerba, M. T.; Lectka, T. Combining Asymmetric Catalysis with Natural Product Functionalization through Enantioselective α-Fluorination. *J. Org. Chem.* **2009**, *75*, 969-971.

(22) Paull, D. H.; Scerba, M. T.; Alden-Danforth, E.; Widger, L. R.; Lectka, T. Catalytic, Asymmetric α-Fluorination of Acid Chlorides: Dual Metal–Ketene Enolate Activation. *J. Am. Chem. Soc.* **2008**, *130*, 17260-17261.

(23) Suzuki, T.; Hamashima, Y.; Sodeoka, M. Asymmetric Fluorination of α-Aryl Acetic Acid Derivatives with the Catalytic System NiCl2-Binap/R3SiOTf/2, 6-Lutidine. *Angew. Chem. Int. Ed.* **2007**, *46,* 5435-5439.

(24) Pihko, P. M. Enantioselective α-Fluorination of Carbonyl Compounds: Organocatalysis or Metal Catalysis? *Angew. Chem. Int. Ed.* **2006**, *45,* 544-547.

(25) Oestreich, M. Strategies for Catalytic Asymmetric Electrophilic α-Halogenation of Carbonyl Compounds. *Angew. Chem. Int. Ed.* **2005**, *44,* 2324-2327.

(26) Muniz, K. Improving Enantioselective Fluorination Reactions: Chiral N-Fluoroammonium Salts and Transition Metal Catalysts. *Angew. Chem. Int. Ed.* **2001**, *40,* 1653-1656.

(27) Pickl, M.; Swoboda, A.; Romero, E.; Winkler, C. K.; Binda, C.; Mattevi, A.; Faber, K.; Fraaije, M. W. Kinetic Resolution of *sec*-Thiols by Enantioselective Oxidation with Rationally Engineered 5-(Hydroxymethyl)furfural Oxidase. *Angew. Chem. Int. Ed.* **2018**, *57*, 2864-2868.

(28) Verho, O.; Backvall, J.-E. Chemoenzymatic Dynamic Kinetic Resolution: A Powerful Tool for the Preparation of Enantiomerically Pure Alcohols and Amines. *J. Am. Chem. Soc.* **2015**, *137*, 3996-4009.

(29) Steinreiber, J.; Faber, K.; Griengl, H. De-racemization of Enantiomers versus De-epimerization of Diastereomers-Classification of Dynamic Kinetic Asymmetric Transformations (DYKAT). *Chem. Eur. J.* **2008**, *14*, 8010-8072.

(30) Persson, B. A.; Larsson, A. L. E.; Le Ray, M.; Backvall, J. E. Ruthenium- and Enzyme-Catalyzed Dynamic Kinetic Resolution of Secondary Alcohols. *J. Am. Chem. Soc.* **1999**, *121*, 1645-1650.

(31) Schober, M.; Faber, K. Inverting Hydrolases and Their Use in Enantioconvergent Biotransformations. *Trends.Biotechnol.* **2013**, *31*, 468-478.

(32) Xu, J.; Hu, Y.; Fan, J.; Arkin, M.; Li, D.; Peng, Y.; Xu, W.; Lin, X.; Wu, Q. Light-Driven Kinetic Resolution of α-Functionalized Carboxylic Acids Enabled by an Engineered Fatty Acid Photodecarboxylase. *Angew. Chem. Int. Ed.* **2019**, *58,* 8474-8478.

(33) Fang, J.; Hait, D.; Head-Gordon, M.; Chang, M. C. Y. Chemoenzymatic Platform for Synthesis of Chiral Organofluorines Based on Type II Aldolases. *Angew. Chem. Int. Ed.* **2019**, *58*, 11841-11845.

(34) Tranel, F.; Haufe, G. Lipase-catalyzed Resolution of 2-Fluorodecanoic Acid. *Tetrahedron: Asymmetry* **2000**, *11*, 889-896.

(35) Bellezza, F.; Cipiciani, A.; Ricci, G.; Ruzziconi, R. On the Enzymatic Hydrolysis of Methyl 2-Fluoro-2-arylpropionates by Lipases. *Tetrahedron.* **2005**, *61,* 8005-8012.

(36) Fukuyama, Y.; Matoishi, K.; Iwasaki, M.; Takizawa, E.; Miyazaki, M.; Ohta, H.; Hanzawa, S.; Kakidani, H.; Sugai, T. Preparative-scale Enzyme-catalyzed Synthesis of (*R*)-α-Fluorophenylacetic Acid. *Biosci. Biotechnol. Biochem.* **1999**, *63,* 1664-1666.

(37) Effenberger, F.; Oßwald, S. Enantioselective Hydrolysis of (*RS*)-2-Fluoroarylacetonitriles using Nitrilase from *Arabidopsis Thaliana*. *Tetrahedron:* **2001**, *12,* 279-285.

(38) Chan, W. Y.; Wong, M.; Guthrie, J.; Savchenko, A. V.; Yakunin, A. F.; Pai, E. F.; Edwards, E. A. Sequence- and Activity-based Screening of Microbial Genomes for Novel Dehalogenases. *Micro. Biotech.* **2010**, *3,* 107-120.

(39) Chan, P. W.; Yakunin, A. F.; Edwards, E. A.; Pai, E. F. Mapping the Reaction Coordinates of Enzymatic Defluorination. *J. Am. Chem. Soc.* **2011**, *133,* 7461-7468.

(40) Kim, T. H.; Mehrabi, P.; Ren, Z.; Sljoka, A.; Ing, C.; Bezginov, A.; Ye, L.; Pomès, R.; Prosser, R. S.; Pai, E. F. The Role of Dimer Asymmetry and Protomer Dynamics in Enzyme Catalysis. *Science* **2017**, *355,* eaag2355.

(41) Mehrabi, P.; Di Pietrantonio, C.; Kim, T. H.; Sljoka, A.; Taverner, K.; Ing, C.; Kruglyak, N.; Pomes, R.; Pai, E. F.; Prosser, R. S. Substrate-Based Allosteric Regulation of a Homodimeric Enzyme. *J. Am. Chem. Soc.* **2019**, *141, 29*, 11540-11556.

(42) Li, Y.; Zhang, R.; Du, L.; Zhang, Q.; Wang, W. Catalytic Mechanism of C-F Bond Cleavage: Insights from QM/MM Analysis of Fluoroacetate Dehalogenase. *Catal. Sci. Technol.* **2016**, *6,* 73-80.

(43) Miranda-Rojas, S.; Fernández, I.; Kästner, J.; Toro-Labbé, A.; Mendizábal, F. Unraveling the Nature of the Catalytic Power of Fluoroacetate Dehalogenase. *ChemCatChem.* **2018**, *10,* 1052-1063.

(44) Miranda-Rojas, S.; Toro-Labbé, A. Mechanistic Insights into the Dehalogenation Reaction of Fluoroacetate/Fluoroacetic Acid. *J. Chem. Phys.* **2015**, *142,* 194301.

(45) Li, Y.; Yue, Y.; Zhang, H.; Yang, Z.; Wang, H.; Tian, S.; Wang, J-b.; Zhang, Q.; Wang, W. Harnessing Fluoroacetate Dehalogenase for Defluorination of Fluorocarboxylic Acids: in Silico and in Vitro Approach. *Environ. Inter.* **2019**, *131,* 104999.

(46) Kurihara, T.; Esaki, N.; Soda, K. Bacterial 2-Haloacid Dehalogenases: Structures and Reaction Mechanisms. *J. Mol. Catal. B: Enzymatic* **2000**, *10,* 57-65.

(47) Wang, J.-b.; Ilie, A.; Yuan, S.; Reetz, M. T. Investigating Substrate Scope and Enantioselectivity of a Defluorinase by a Stereochemical Probe. *J. Am. Chem. Soc.* **2017**, *139,* 11241-11247.

(48) Kamachi, T.; Nakayama, T.; Shitamichi, O.; Jitsumori, K.; Kurihara, T.; Esaki, N.; Yoshizawa, K. The Catalytic Mechanism of Fluoroacetate Dehalogenase: a Computational Exploration of Biological Dehalogenation. *Chem. Eur. J.* **2009**, *15*, 7394-7403.

(49) Mehrabi, P.; Schulz, E. C.; Dsouza, R.; Müller-Werkmeister, H. M.; Tellkamp, F.; Miller, R. D.; Pai, E. F. Time-resolved Crystallography Reveals Allosteric Communication Aligned with Molecular Breathing. *Science*, **2019**, *365*, 1167-1170.

(50) Claeyssens, F.; Harvey, J. N.; Manby, F. R.; Mata, R. A.; Mulholland, A. J.; Ranaghan, K. E.; Werner, H. J. High‐accuracy Computation of Reaction Barriers in Enzymes. *Angew. Chem. Int. Ed.* **2006**, *45*, 6856–6859.

(51) Senn, H. M.; Thiel, W. QM/MM Methods for Biomolecular Systems. *Angew. Chem. Int. Ed.* **2009**, *48*, 1198–1229.

(52) Shaik, S.; Cohen, S.; Wang, Y.; Chen, H.; Kumar, D.; Thiel, W. P450 Enzymes: Their Structure, Reactivity, and Selectivity⊠ Modeled by QM/MM Calculations. *Chem. Rev.* **2010**, *110*, 949–1017.

(53) Lu, Q.; Song, J.; Wu, P.; Mechanistic Insights into the Directing Effect of Thr303 in Ethanol Oxidation by Cytochrome P450 2E1. *ACS Catal.* **2019**, *9*, 4892–4901.

(54) Wang, B.; Cao, Z.; Rovira, C.; Fenton-derived OH Radicals Enable the MPnS Enzyme to Convert 2-Hydroxyethylphosphonate to Methylphosphonate: Insights from Ab Initio QM/MM MD Simulations. *J. Am. Chem. Soc.* **2019**, *141*, 9284–9291.

(55) Wu, P.; Fan, F.; Song, J.; Theory Demonstrated a "Coupled" Mechanism for O2 Activation and Substrate Hydroxylation by Binuclear Copper Monooxygenases. *J. Am. Chem. Soc.* **2019**, *141,* 19776–19789.

(56) Murdoch, J. R. What is the Rate-limiting Step of A Multistep Reaction? *J. Chem. Educ.***1981**, *58*, 32-36.

(57) Kozuch, S.; Martin, J. M. L. The Rate-Determining Step is Dead. Long Live the Rate-Determining State! *Chemphyschem*, **2011**, *12*, 1413-1418.

(58) Gadda, G.; Sobrado, P. Kinetic Solvent Viscosity Effects as Probes for Studying the Mechanisms of Enzyme Action. *Biochemistry*, **2018**, *57*, 3445-3453.

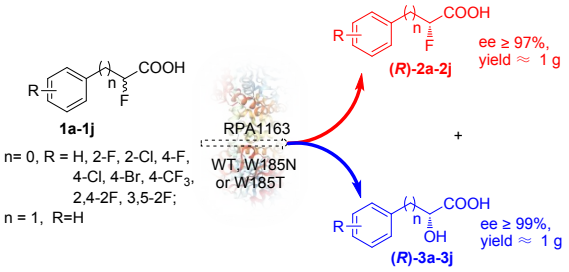

For Table of Contents Only